Cancer Medicine

WILEY

Cancer Medicine Open Access

RESEARCH ARTICLE OPEN ACCESS

Multi-Transcriptomic Analysis Reveals That EREG-Driven TME Crosstalk Defines Anti-EGFR Response in Colorectal Cancer

Atsuki Taniguchi[1] | Shunsuke Kagawa[1] | Shohei Nogi[1] | Tomohiko Yagi[1] | Nobuhiko Kanaya[1] | Shinji Kuroda[1] | Satoru Kikuchi[1] | Yoshihiko Kakiuchi[1,2] | Hiroshi Tazawa[1,3] | Toshiyoshi Fujiwara[1]

[1]Department of Gastroenterological Surgery, Graduate School of Medicine, Dentistry and Pharmaceutical Sciences, Okayama University, Okayama, Japan | [2]Minimally Invasive Therapy Center, Okayama University Hospital, Okayama, Japan | [3]Center for Innovative Clinical Medicine, Okayama University Hospital, Okayama, Japan

Correspondence: Atsuki Taniguchi (pe9w3u9l@s.okayama-u.ac.jp)

Received: 21 August 2025 | **Revised:** 11 March 2026 | **Accepted:** 13 April 2026

Keywords: cell–cell interaction | colorectal cancer | EGFR inhibitor eligibility | Epiregulin (EREG) | tumor microenvironment

ABSTRACT

Sidedness influences colorectal cancer (CRC) prognosis and treatment response, yet the mechanism dictating differential EGFR inhibitor (EGFRI) sensitivity is unclear. This study investigated the tumor microenvironment (TME) in relation to EGFRI eligibility—clinically defined by factors such as tumor sidedness (e.g., left-sided), RAS/BRAF wild-type status, and microsatellite stability (MSS)—using integrated single-cell RNA sequencing (scRNA-seq), with bulk RNA-seq and spatial transcriptomics validation. We found cancer cell features reflected EGFRI eligibility more strongly than sidedness. EGFRI eligible tumors exhibited high Epiregulin (EREG) expression by cancer cells. Cell interaction analysis revealed a specific "EREG/EGFR/CSF axis" in EGFRI eligible CRC: EREG derived from cancer cell stimulates EGFR-expressing non-myCAF subtypes of cancer-associated fibroblasts (CAFs), which signal via CSF to M1/M2-like Tumor-Associated Macrophages/Monocytes (TAM/TAMo), potentially promoting M2 polarization. Spatial analysis confirmed the proximity of these interacting cell populations and localized EGFR pathway activation near cancer cells specifically in eligible tumors. This study provides a TME-centric view of EGFRI eligibility, identifying a key intercellular communication network driving differential responses. These findings suggest TME features could offer more precise patient stratification than sidedness alone, potentially improving CRC therapeutic strategies.

1 | Introduction

Colorectal Cancer (CRC) is a major global health concern, ranking third in diagnosis and fourth in cancer-related mortality [1]. Characterizing its biological heterogeneity for more precise therapeutic strategies is a pressing challenge. Significant clinical and molecular differences exist depending on primary tumor origin in the right or left colorectum (tumor "sidedness") [2–4]. Right-sided colon cancer (RCC) derives from the midgut, while left-sided colorectal cancer (LCRC) originates from the hindgut. It has been suggested that these differences in embryological origin and gut microbiota composition significantly influence variations in gene mutation profiles and the TME [5].

Multiple cohort studies of advanced CRC report poorer prognosis for RCC versus LCRC [6, 7]. Similarly, treatment outcomes for colorectal liver metastases (CRLM) vary by primary tumor location, with right-sided tumors showing greater treatment resistance [8]. Considering these clinical features, CRC sidedness has emerged as a crucial biomarker for guiding treatment decisions and is widely utilized, particularly for predicting the efficacy of epidermal growth factor receptor

inhibitors (EGFRI) [9]. For the treatment of metastatic colorectal cancer (mCRC), different therapeutic approaches are recommended for right-sided versus left-sided tumors in patients with microsatellite stable (MSS), RAS wild-type, and BRAF wild-type [10, 11].

While RAS wild-type LCRC exhibits high sensitivity to EGFRI [12], the underlying molecular mechanisms remain incompletely understood. Recent studies suggest that the expression levels of EGFR ligands secreted by tumor cells, such as epiregulin (EREG) and amphiregulin (AREG), may serve as potential novel biomarkers for predicting response to EGFR inhibitor therapy [13, 14]. Furthermore, variations in the TME are known to influence the response to anti-EGFR therapy [15, 16]. This suggests that responsiveness to EGFRI may be governed by complex interactions among tumor cells, immune cells, and stromal cells, extending beyond simple primary tumor sidedness.

Therefore, in this study, we performed an integrative analysis using transcriptome such as scRNA-seq, bulk RNA-seq, and spatial transcriptomics. Specifically, our aim was to comprehensively characterize the differences in cancer cells, immune cells, and fibroblasts between right-sided and left-sided primary tumors, and subsequently identify specific TME features associated with responsiveness to EGFRI. In this study, we define "EGFRI eligible" tumors as those with a left-sided primary origin, RAS and BRAF wild-type status, and MSS, representing the patient population most likely to benefit from EGFRI therapy.

Our results revealed that these "EGFRI eligible" patient tumors, EREG expressed by CRC cells, initiate the formation of a specific interaction network, termed the "EREG/EGFR/CSF axis," involving cancer cells, fibroblasts, and myeloid cells. Furthermore, our findings suggest that specific subtypes of fibroblasts and myeloid cells are critically involved in establishing this interaction network.

In summary, this study provides a comprehensive analysis of EGFRI sensitivity in CRC from the perspective of the TME, aiming to propose a more refined and clinically relevant classification framework that transcends simple primary tumor sidedness. The findings of this research are anticipated to overcome the limitations of conventional classifications based primarily on sidedness, potentially leading to a new paradigm for a deeper understanding of CRC heterogeneity.

2 | Material and Methods

2.1 | Data Collection and Patient Cohort

scRNA-seq data from human CRC tissues and adjacent normal tissues, with clinical information, were sourced from two public datasets. The first dataset comprised five cohorts (KUL3, KUL5, CRC-SG1, CRC-SG2, and SMC) obtained from Synapse (ID: syn26844071). The second dataset (GSE200997 cohort) was obtained from GEO (accession: GSE200997). In this dataset, only specific samples were selected for our primary analysis to strictly fulfill the criteria for evaluating EGFRI eligibility (MSS and BRAF V600E wild-type). In total, for our primary analysis, we selected 109 MSS, BRAF V600E wild-type tumor samples and 35 normal samples for which sidedness and RAS mutation metadata were available. The use of all data was in accordance with the policies of the relevant institutional review boards for each respective research project.

2.2 | scRNA-Seq Data Processing, Quality Control, and Integration

Initial quality control (QC) of the single-cell data was performed in the original studies prior to our analysis. Our study began with these pre-processed datasets.

For the five-cohort dataset (KUL3, KUL5, CRC-SG1, CRC-SG2, SMC), rigorous cell-type-specific QC had been applied as previously described. This included the removal of doublets using DoubletFinder and filtering cells based on cell-type-specific cutoffs for the number of detected genes and the percentage of mitochondrial reads (e.g., for epithelial cells, NODG <2200 or >7500, and mitochondrial percentage $<3.0\%$ or $>23.0\%$ were excluded). For the GSE200997 dataset, cells with a mitochondrial gene percentage exceeding 25% had been removed, and doublets were identified and excluded using the DoubletFinder package. The pre-processed data from these cohorts were then integrated for downstream analysis using the Seurat package (v5.2.1). Epithelial and non-epithelial cell data from the EGA/Synapse datasets were merged, and subsequent data processing followed a standard Seurat workflow for integration and clustering.

2.3 | CNV Estimation

To assess the malignant potential of epithelial cells, CNV profiles were inferred using the inferCNV R package (v1.22.0; https://github.com/broadinstitute/InferCNV). Raw UMI count matrices from epithelial cells were used as input, with normal epithelial cells serving as the reference.

2.4 | Pseudobulk RNA-Seq Analysis

UMI counts were aggregated per sample for each major cell type using AggregateExpression function. Samples with low cell counts (epithelial: <50 cells; fibroblasts: <50 cells; myeloid: <50cells; T cell: <100 cells) were excluded. The resulting count matrices were processed using DESeq2 (v1.46.0) for variance-stabilizing transformation. Batch effects across datasets were corrected using ComBat_seq from the sva package (v3.54.0), except for T cells where removeBatchEffect from the limma package (v3.62.2) was used.

2.5 | GSEA and Pathway Activity Scoring (AUCell)

Biological pathway activity was assessed using GSEA and AUCell. GSEA was performed using the clusterProfiler package (v4.14.4) on ranked gene lists derived from DEG analyses. Gene sets from MSigDB and custom literature-derived gene sets (e.g., M1/M2 subtype signatures, CAF subtype signatures) were used. Normalized Enrichment Scores (NES) were visualized using heatmaps generated with pheatmap (v1.0.12). For Visium data,

pathway activity per spot was scored using the AUCell package (v1.28.0).

2.6 | Cell–Cell Interaction Analysis

Cell–cell communication networks were inferred using CellChat (v2.1.2) and NicheNet (v2.1.7). For CellChat analysis, the standard workflow was followed; specifically, communication probabilities were computed using the default triMean method, and filtering was applied with min.cells = 10. For NicheNet, ligand activities predicting target gene expression in receiver cells were computed using the predict_ligand_activities function, based on DEG analysis between conditions.

2.7 | Pseudotime Trajectory Analysis

Monocle3 (v1.3.7) was applied to the previously defined macrophage/monocyte subset. Trajectory graphs were learned using learn_graph function, and pseudotime was calculated using order_cells function.

2.8 | TCGA Data Analysis and CIBERSORTx Deconvolution

To validate cell type compositions in bulk tissue, TCGA COAD and READ datasets were analyzed. BRAF V600E wild-type cases were selected and stratified into EGFRI eligibility groups based on sidedness and KRAS mutation status. Signature matrices were generated from the scRNA-seq data. These matrices, along with TCGA bulk RNA-seq data, were used as input for CIBERSORTx to estimate cell type fractions in each TCGA sample. Estimated proportions were compared between EGFRI eligibility groups using the Wilcoxon test.

2.9 | Spatial Transcriptomics Analysis

Spatial transcriptomics data were obtained via Zenodo (DOI: 10.5281/zenodo.15298305). Pathologist annotations, provided by expert pathologists on the author team, were used to inform the analysis. Cell type composition per spot was estimated using CytoSPACE with the integrated scRNA-seq data as a reference. Tumor proximity analysis focused specifically on spots annotated by pathologists as "stroma_fibroblastic_IC", representing fibroblastic stroma with immune cell (IC) infiltration. The distance from each "stroma_fibroblastic_IC" spot to the nearest annotated tumor spot was calculated. The spots were classified as "Near" or "Far" using the median distance threshold. AUCell pathway scores were compared between proximity groups. The $\log_2$ fold change of the mean AUCell score of the "Near" group relative to the "Far" group $\left(\mathrm{LFC} = \log_2\left(\frac{\mathrm{Mean}(\mathrm{AUCell}_{\mathrm{Near}})}{\mathrm{Mean}(\mathrm{AUCell}_{\mathrm{Far}})}\right)\right)$ was then computed to quantify the differential pathway enrichment associated with tumor proximity. Additionally, to validate these findings, an independent Visium cohort (GSE226997) was analyzed (Figure S6). Because pathologist annotations were unavailable for this cohort, stromal spots were computationally defined based on module scores for fibroblasts and myeloid cells, excluding regions with high epithelial or smooth muscle scores. Tumor proximity was similarly evaluated.

3 | Results

3.1 | Integrative Analysis of scRNA-Seq Constructed a Comprehensive Atlas of Cellular Diversity in CRC

We collected 144 samples (109 tumor tissues, 35 adjacent normal tissues) from six public scRNA-seq datasets, focusing on BRAF wild-type, MSS cases where primary tumor sidedness information was available (Figure 1A; Table S1). This design allowed for analysis considering eligibility for EGFRI therapy.

Next, we integrated scRNA-seq data, annotating major cell types (Figure 1B). A heatmap of top 6 marker DEGs showed distinct cell-type-specific signatures, confirming appropriate annotation (Figure 1C). We also evaluated the cell type proportions and EREG expression levels per dataset. While there was some variance in EREG expression across datasets, we confirmed that no specific dataset predominantly skewed the results (Figure S1A,B).

The integrated scRNA-seq data were visualized to evaluate associations with clinical information. When cells were colored based on tumor sidedness (Left vs. Right), RAS mutation status (Wild-type vs. Mutant), and EGFRI eligibility (EGFRI eligible vs. EGFRI ineligible), no major biases were observed in the overall cell distribution (Figure 1D–F).

3.2 | EGFRI Eligibility Reflects Cancer Cell Characteristics More Than Sidedness

We exploratorily analyzed the molecular differences among cancer cells in CRC. We identified *EPCAM*-positive epithelial cells and extracted 33,180 cells derived from tumor tissues for re-integration. As a result, cancer cells were classified into six major clusters (Figure 2A). When assessing genomic differences at the cancer cell level using copy number variation (CNV) analysis with inferCNV, LCRC showed more widespread chromosomal instability (CIN), with clear differences observed particularly in regions 1p, 13q, 14q, 18pq, and 20pq (Figure 2B), consistent with previous reports [17].

Furthermore, DEG analysis based on sidedness identified genes like PRAC1 (characteristic of rectum, distal colon, and prostate) and EREG known as one of the EGFR ligands on the left side. On the right side, REG4, ANXA1, and KRT7 were detected (Figure 2C). ANXA1 is involved in inflammatory responses and immunosuppression and has been linked to poor prognosis [18]. KRT7 is involved in cancer progression and metastasis and may be related to the serrated neoplasia pathway known to be associated with RCC [19, 20]. As REG4 is also known as a characteristic gene for mucinous carcinoma, we examined the expression of mucinous carcinoma-related genes (REG4, SPINK4, FCGBP, MUC2). These were enriched and highly expressed in cluster 2, suggesting that cluster 2 represents a cell population with mucinous carcinoma-like characteristics (Figure S2A).

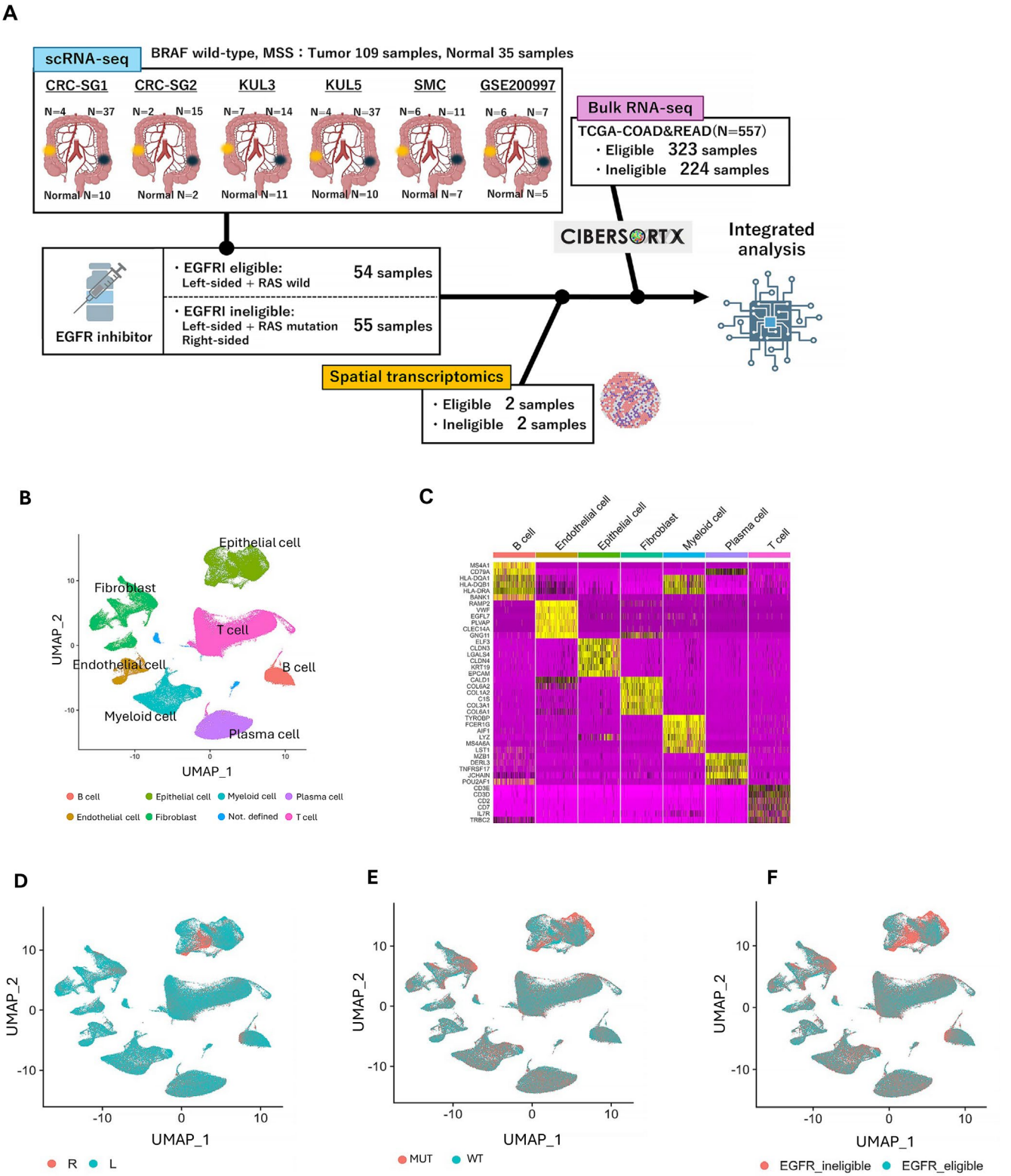

FIGURE 1 | Study design and integration of public scRNA-seq datasets. (A) Schematic overview of the study design created with BioRender.com. EGFRI-eligible tumors are defined as a left-sided primary origin, RAS/BRAF wild-type status, and microsatellite stability (MSS). (B) Integrated scRNA-seq data with cell types annotated by DEGs. (C) Heatmap of top 6 marker genes per cell type. (D–F) UMAP of integrated data colored by Sidedness (D), RAS status (E), and EGFRI eligibility (F).

To evaluate the differences in the overall transcriptome profiles of cancer cell populations, we created pseudo-bulk data by averaging gene expression across cancer cells for each sample and performed Principal Component Analysis (PCA). When samples were compared by tumor sidedness and EGFRI eligibility, the classification by EGFRI eligibility appeared to more fundamentally reflect the differences in cancer cell gene expression profiles than the classification by tumor sidedness (Figure 2D).

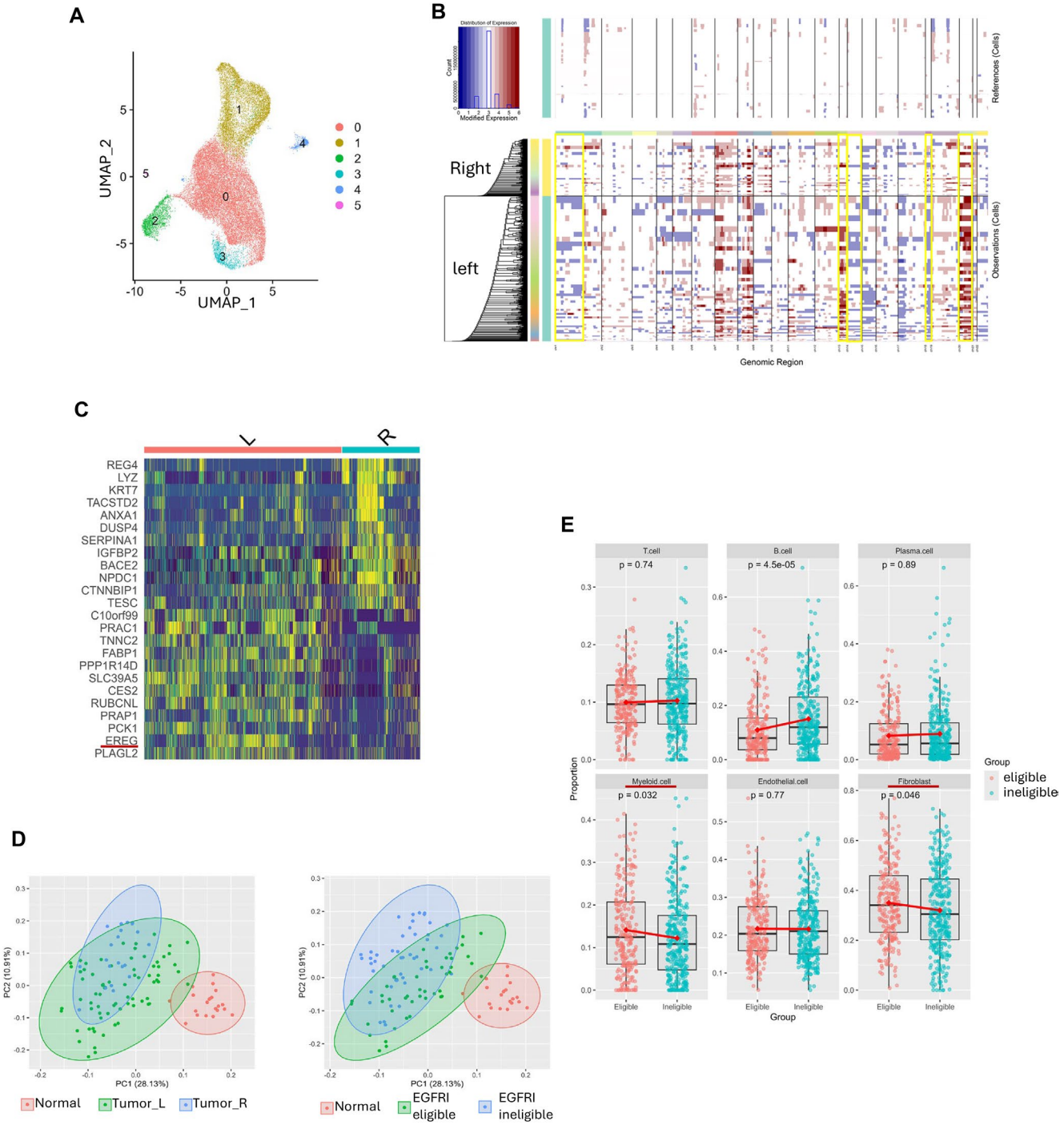

FIGURE 2 | "EGFRI eligibility" better stratifies cancer cell characteristics than "Sidedness." (A) Re-integration and UMAP of 33,180 tumor-derived EPCAM-positive cells. (B) Cancer cell CNV profiles via inferCNV, stratified by Sidedness. Red: Putative gains; blue: Putative losses, relative to reference. Yellow boxes highlight altered chromosomal regions. (C) Heatmap of top 12 DEGs by Sidedness. (D) Principal component analysis (PCA) of pseudo-bulk profiles of cancer cells. Samples are colored by sidedness (left panel), EGFRI eligibility (middle panel), and dataset origin (right panel). (E) CIBERSORTx estimation of non-cancer cell abundance in TCGA-COAD/READ by EGFRI eligibility. Statistical analysis was performed using a two-sided Wilcoxon rank-sum test, and *p*-values are shown.

Furthermore, to investigate the relationship between EGFRI eligibility and the overall TME, we estimated the cellular composition of TCGA bulk RNA-seq data using CIBERSORTx [21]. The results revealed that EGFRI ineligible cases had significantly lower estimated proportions of myeloid cells and fibroblasts compared to EGFRI eligible cases (Figure 2E). This indicates that EGFRI eligibility is associated with differences in TME cell composition ratios. On the other hand, when performing pseudo-bulk PCA on the major TME constituent cells (T cells, myeloid cells, fibroblasts) using our scRNA-seq data, no clear separation based on transcriptomes (qualitative difference) was observed according to EGFRI eligibility (Figure S2B–D). This

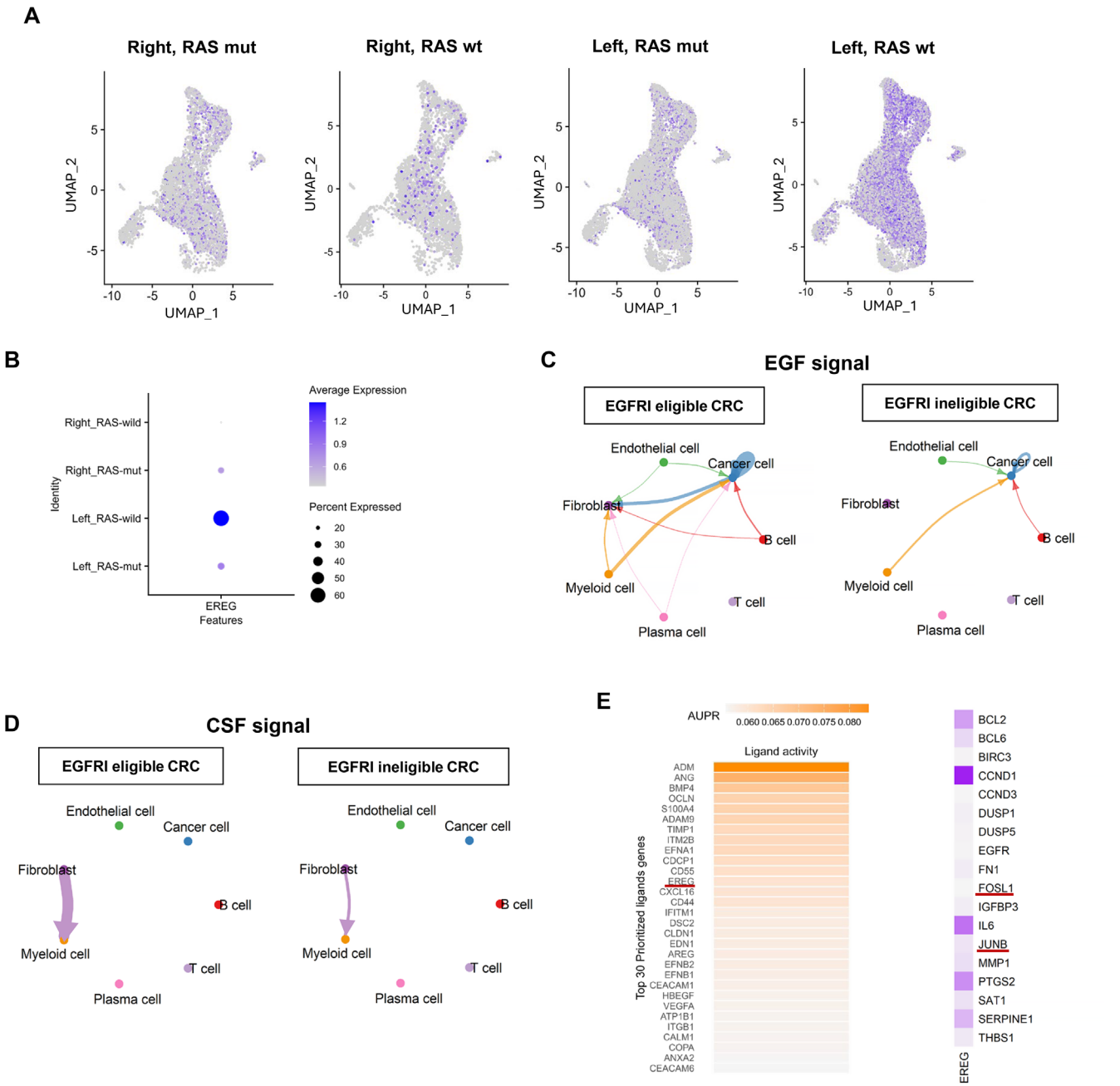

FIGURE 3 | EREG-mediated intercellular signaling network analysis in EGFRI eligible colorectal cancer. (A) FeaturepPlot of comparison of EREG expression in cancer cells stratified by RAS mutation status and sidedness. (B) Dot plot of EREG-expressing cancer cell proportions, stratified by RAS status and sidedness. (C, D) Network diagrams showing signaling strength between cell types in the EGF signaling pathway (B) and CSF signaling pathway (C) for EGFRI eligible and EGFRI ineligible cases. Line thickness indicates signal strength (weight). (E) NicheNet analysis predicting downstream effects from cancer cells to fibroblasts. Top 30 predicted active ligands potentially involved in signaling from cancer cells to fibroblasts in EGFRI eligible cases (left panel). Potential target genes regulated by cancer cell-derived EREG within fibroblasts (right panel).

suggests that while EGFRI eligibility may not drastically alter the overall transcriptome of these cells, it might influence the TME through changes in cellular composition.

3.3 | EREG Plays a Central Role in the Cell–Cell Interaction Network in EGFRI Eligible CRC

EREG, which showed a tendency for higher expression in LCRC, is also attracting attention as a candidate predictive biomarker for EGFRI sensitivity [14, 22, 23]. Therefore, we conducted a detailed analysis of EREG expression in relation to EGFRI eligibility and the cell–cell communication involved.

EREG expression in cancer cells was significantly upregulated in the EGFRI eligible group, also ranking as a top upregulated gene based on EGFRI eligibility alone (Figure 3A,B; Figure S3A). In contrast, other known EGFR ligands (AREG, EGF, TGFA, BTC, EPGN, HBEGF) did not show such a clear association with EGFRI eligibility (Figure S3B). These findings strongly suggest a key role for EREG expressed by cancer cells in EGFRI eligible CRC.

Next, we comprehensively analyzed the changes in cell–cell communication due to differences in EGFRI eligibility using CellChat [24, 25]. In EGFRI eligible cases, fibroblasts and myeloid cells were the key players in this increase, acting as the primary signal senders and receivers, respectively. Among these interactions, signaling from fibroblasts to myeloid cells was markedly enhanced (Figure S3C).

We analyzed these changes in cell–cell communication at the level of individual signaling pathways for each cell type. Focusing first on signals from cancer cells to fibroblasts, an enhancement of the EGF signaling pathway was observed in EGFRI eligible cases (Figure S3D). Network diagrams showed that while EGF signaling primarily functions as an autocrine loop among cancer cells in ineligible cases, signaling from cancer cells to fibroblasts newly emerged in eligible cases (Figure 3C). To comprehensively visualize the specific ligand-receptor pairs driving these interactions and their probabilities, we provided bubble plots focusing on the EGF and CSF pathways (Figure S3E). Next, examining the signaling pathways most enhanced from fibroblasts to myeloid cells in eligible cases identified enhancements in the CSF signaling pathway and the NOTCH signaling pathway (Figure S3D). As reports on NOTCH signaling from fibroblasts to myeloid cells are limited, we focused on the CSF signaling pathway (Figure 3D). These findings suggest a potential cascading interaction in EGFRI eligible cases: cancer cells (high EREG) act on fibroblasts via enhanced EGF signaling, and these fibroblasts, in turn, act on myeloid cells via enhanced CSF signaling.

To further test this hypothesis, we used NicheNet [26] to predict the downstream effects of signaling from cancer cells to fibroblasts in EGFRI eligible cases. The results ranked EREG highly as a ligand acting from cancer cells onto fibroblasts and predicted FOSL1 and JUNB, components of the AP-1 complex, as potential transcription factors activated within fibroblasts upon receiving EREG signals (Figure 3E). AP-1 transcription factors are known to be activated downstream of EGFR signaling and induce the expression of CSF family genes (CSF1/CSF2) [27–29]. Therefore, the integrated analysis of CellChat and NicheNet suggests the potential formation of a specific "EREG/EGFR/CSF axis" in EGFRI eligible CRC, where cancer cell-derived EREG activates the AP-1 pathway via EGFR in fibroblasts, consequently enhancing CSF production and secretion from fibroblasts, which then acts on myeloid cells.

3.4 | Interaction Between Cancer Cells and Fibroblasts in EGFRI Eligible CRC Is Mediated by Non-myCAFs

The findings suggested an interaction network involving EREG-mediated communication between cancer cells, fibroblasts, and immune cells in EGFRI eligible CRC. To identify which fibroblast subtype is involved in this interaction, focusing on the heterogeneity of fibroblasts playing a central role in this axis, we performed sub-clustering analysis.

First, we identified the fibroblast cluster from the integrated data and confirmed marker gene expression (Figure S4A). Fibroblasts derived from tumor tissues were extracted as CAFs and subjected to re-integration and re-clustering. As a result, CAFs were primarily classified into four subtypes. Based on previously reported markers [30], CAFs were classified into myCAF, iCAF, as well as SOX6+Fib and ADAMDEC1+Fib (Figure S3A,B). Comparing the proportions of CAF subtypes based on EGFRI eligibility revealed that myCAFs were proportionally higher in the EGFRI ineligible group, while iCAFs were higher in the eligible group (Figure 4A). This trend was reproduced in our CIBERSORTx analysis of bulk RNA-seq data, which confirmed consistent CAF subtype ratios (Figure 4B).

To elucidate the biological characteristics of each identified CAF subtype, GSEA was performed using signature gene sets for CAF subtypes reported previously [30–33]. The results showed that SOX6+ Fibs were enriched for pathways related to tissue remodeling, such as bone morphogenetic protein (BMP) production, while ADAMDEC1+Fibs were enriched for pathways involved in immune cell recruitment, such as gene sets related to the chemokine CCL8. Pathways related to myCAF and iCAF were not enriched, suggesting that these subtypes may possess tissue-specific or distinct functional roles within the TME of CRC, such as BMP production or CCL8-mediated immune cell recruitment (Figure 4C).

We then used CellChat to analyze which CAF subtype is responsible for the enhanced EGF signaling from cancer cells to fibroblasts observed in EGFRI eligible cases. The results showed that interactions via EGF signaling with cancer cells were strongly detected primarily in SOX6+ Fibs and iCAFs (Figure 4D). Since EGFR expression on the CAF side is essential for this interaction, we examined EGFR expression levels in each subtype. SOX6+ Fibs and iCAFs expressed EGFR, whereas myCAFs showed nearly absent EGFR expression (Figure 4E). These results strongly suggest that the EGF signal (including EREG) originating from cancer cells in EGFRI eligible cases is received by EGFR-expressing non-myCAFs (SOX6+ Fibs and iCAFs).

From these results, it became clear that within the "EREG/EGFR/CSF axis" in EGFRI eligible cases, the non-myCAFs expressing EGFR receive the EGF signal (EREG) from cancer cells, while myCAFs, which are increased in EGFRI ineligible cases, are not directly involved in this interaction.

3.5 | Monocyte/Macrophage Lineage Cells Are Classified Into Functionally Distinct Subtypes, and CSF Signaling Is Associated With M2-Like Differentiation

We analyzed myeloid cells, presumed receivers of CSF signals from fibroblasts in the "EREG/EGFR/CSF axis," for subtype identification, functional characteristics, and association with EGFRI eligibility. CD68-positive cells were re-clustered (Figure 5A). Our analysis then focused specifically on Tumor-Associated Macrophages/Monocytes (TAM/TAMo), as CSF signaling is crucial for their development [34]. TAM/TAMo populations were specifically selected based on the expression of characteristic DEGs, including SPP1, CD163, and CSF1R.

Based on their distinct roles in CellChat-inferred EGF and CSF signaling pathways (as senders and receivers, respectively), we sub-clustered TAM/TAMo into three main subtypes:

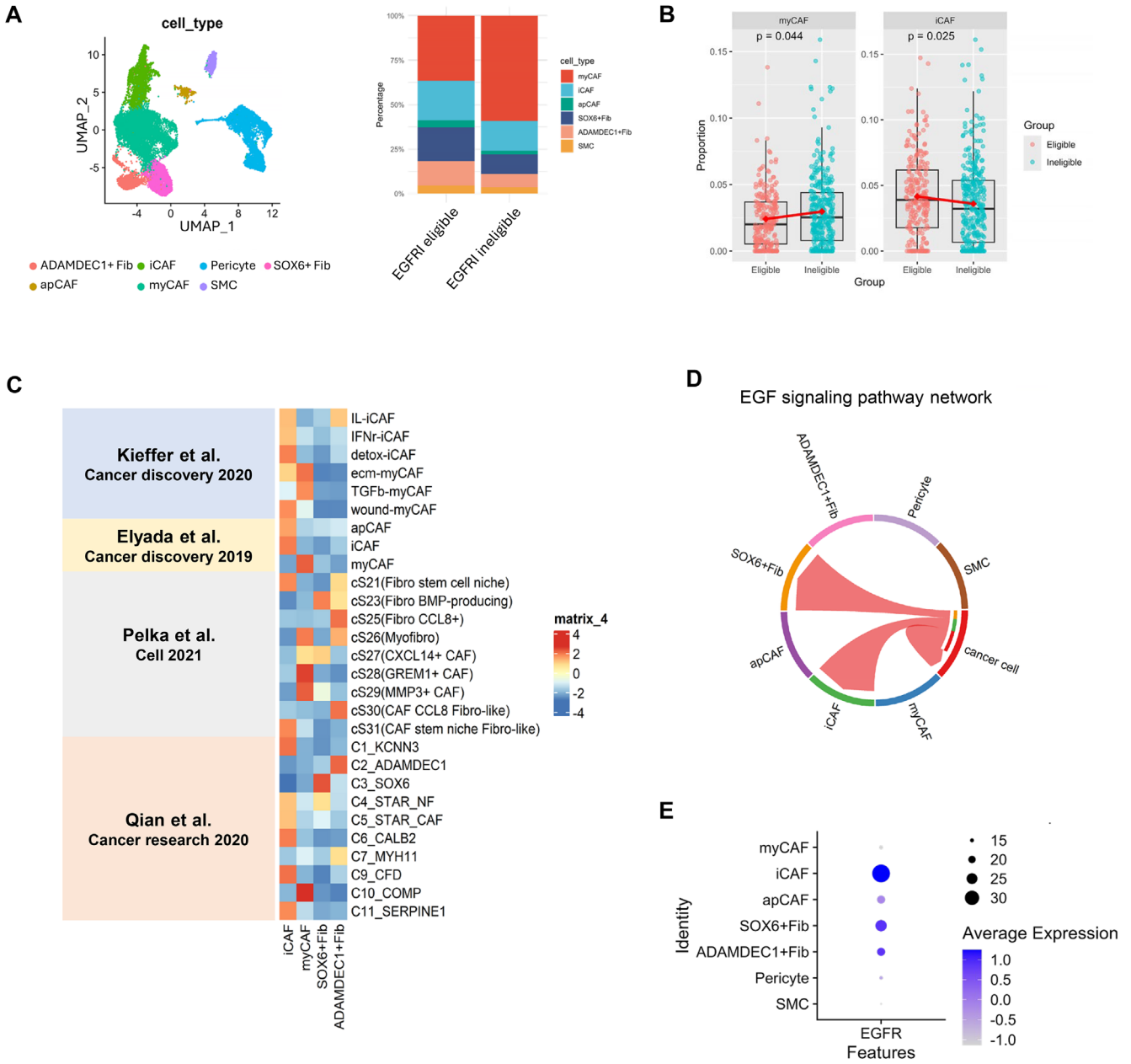

FIGURE 4 | Classification of CAF subtypes and analysis of EGF pathway-mediated interactions with cancer cells in EGFRI eligible cases. (A) Identification of CAF subtypes from tumor tissues (left panel). Stacked bar plot showing the abundance of each CAF subtype stratified by EGFRI eligibility (right panel). (B) Estimated abundance of myCAF and iCAF subtypes in bulk RNA-seq data (TCGA-COAD/READ) using CIBERSORTx. Comparison based on EGFRI eligibility using a two-sided Wilcoxon rank-sum test; *p*-values are shown. (C) Biological interpretation of each CAF subtype using GSEA with gene sets characteristic of previously reported CAF subtypes. (D) CellChat analysis of EGF signaling-mediated intercellular interactions between CAF subtypes and cancer cells in EGFRI eligible cases. Interaction strength is shown. (E) Dot plot showing the EGFR expression in each CAF subtype.

"EGF-TAM/TAMo," "CSF-TAM/TAMo," and "Intermediate-TAM/TAMo" (Figure 5B,C).

GSEA was performed to elucidate the biological characteristics of these subtypes (Figure 5D). The "Intermediate-TAM/TAMo" were enriched for immune activation pathways, including M1-like macrophage signatures [35], inflammatory responses, and antigen presentation. In contrast, "CSF-TAM/TAMo" were enriched for tissue repair and immunosuppression pathways, such as M2-like macrophage signatures [35], and extracellular matrix (ECM) association. Based on these functional profiles and known marker expression (Figure S5A,B), we interpreted these subtypes as progenitor-like TAMo (the "EGF" subtype), classically activated M1-like TAMs (the "Intermediate" subtype), and alternatively activated M2-like TAMs (the "CSF" subtype).

Finally, Monocle3 pseudotime analysis inferred a differentiation trajectory from TAMo, through M1-like TAMs, towards M2-like TAMs (Figure 5E). The root node was set at the cluster

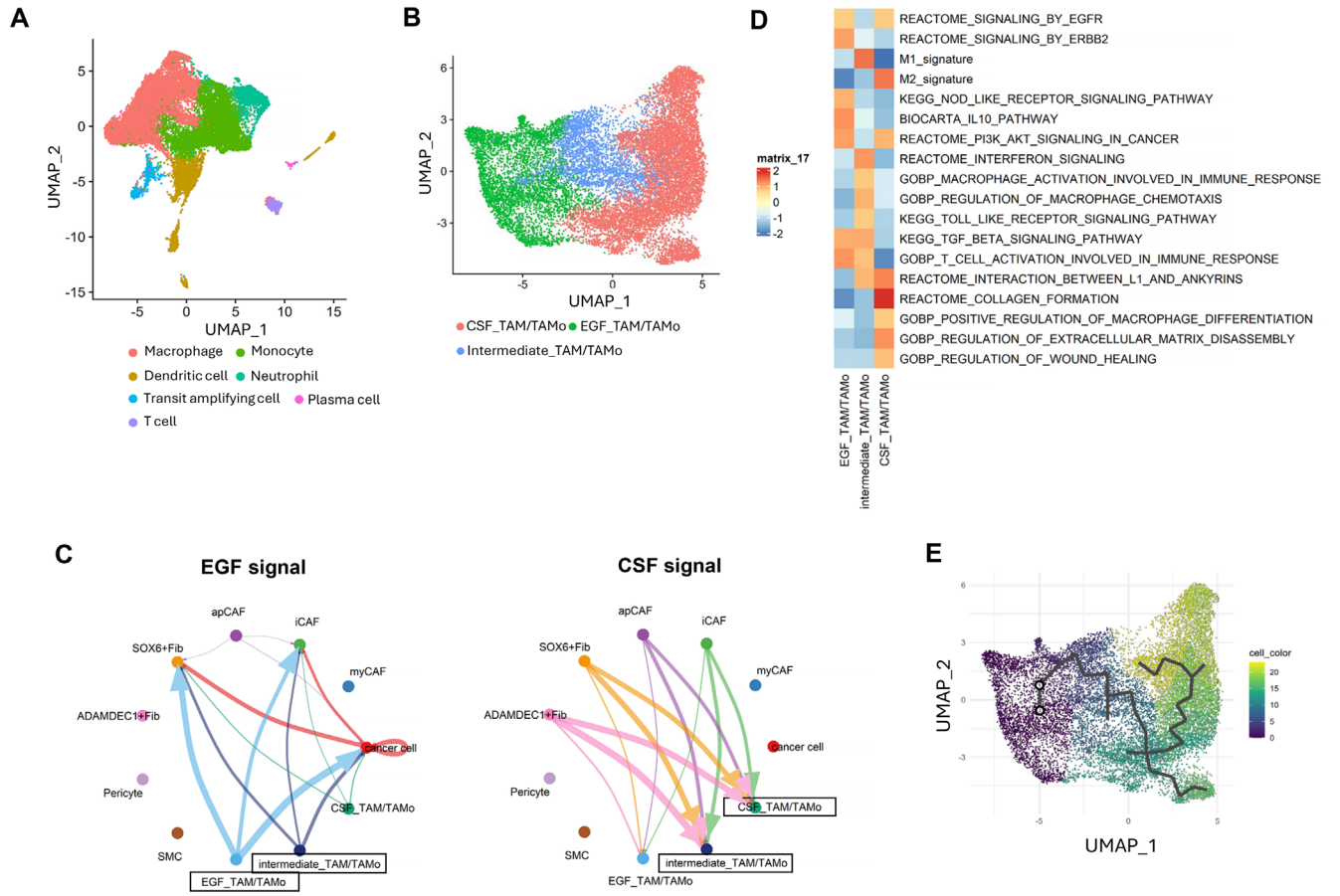

FIGURE 5 | Monocyte/macrophage lineage cells are classified into functionally distinct subtypes based on their involvement in EGF/CSF signaling. (A) UMAP showing re-integrated and clustered CD68-positive cells derived from tumor tissues, with annotations. (B) UMAP showing re-clustered tumor-associated macrophages and monocytes (TAM/TAMo) classified based on their involvement in EGF and CSF signaling pathways. Three subtypes are shown. (C) CellChat analysis of intercellular interaction networks. EGF signaling from cancer cells and CAF subtypes to each TAM/TAMo subtype (left panel). CSF signaling from cancer cells and CAFs to each TAM/TAMo subtype. Interaction strength is shown (right panel). (D) GSEA results for each TAM/TAMo subtype with M1/M2-like signatures and related pathways. (E) Pseudotime trajectory analysis of TAM/TAMo using Monocle3. Arrows indicate the inferred direction of differentiation/polarization.

maintaining classical monocyte features (e.g., S100A8 expression), representing the biological origin of differentiation. Since CSF signaling, particularly CSF1, is known to induce M2-like differentiation of macrophages [36], this trajectory suggests that CSF signals from CAFs may promote the differentiation of TAMs into an immunosuppressive M2-like state.

3.6 | Validation of the EREG/EGFR/CSF Axis in the Tissue Spatial Context Using Spatial Transcriptomics

Our scRNA-seq analysis previously suggested an "EREG/EGFR/CSF axis" in EGFRI-eligible CRC, where cancer cell-derived EREG acts on non-myCAFs, which in turn signal to M1/M2-like TAMs via CSF. To validate this axis and map its spatial organization, we utilized Visium spatial transcriptomics.

Representative EGFRI eligible and ineligible samples were analyzed (Table S2), integrating H&E images (Figure 6A) with gene expression per 55 μm spot. Consistent with scRNA-seq, spatial EREG expression was high in tumor regions of eligible cases but markedly lower in ineligible ones (Figure 6B).

CytoSPACE [37], using our scRNA-seq atlas as a reference, estimated spot cellular composition. This showed TAMo were nearly absent in the EGFRI ineligible case (Figure S6A). Fibroblasts and myeloid cells often co-localized in cancer-devoid stromal regions in both case types (Figure S6B).

To investigate whether these cell–cell interactions occur between spatially proximal cells, we extracted spots where stromal and immune cells co-exist (Stroma+Immune spots) based on pathologist annotation. These spots were classified into "Near spots" and "Far spots" based on their distance to nearby cancer cells (Figure 6C), and their transcriptome profiles were compared. We then compared their pathway activities by calculating the $\log_2$ fold change of AUCell-derived scores (Near vs. Far). In the EGFRI eligible case, this analysis revealed a specific upregulation of the EGFR signaling pathway in Near spots. In contrast, the EGFRI ineligible case did not show a prominent increase in EGFR pathway activity; instead, it exhibited an enrichment of other various cancer-related pathways in Near spots relative to Far spots (Figure 6D). To ensure the robustness of these findings, we validated this spatial dynamic using an independent spatial transcriptomics cohort (GSE226997; Figure S6C,D), which successfully reproduced the marked EREG expression

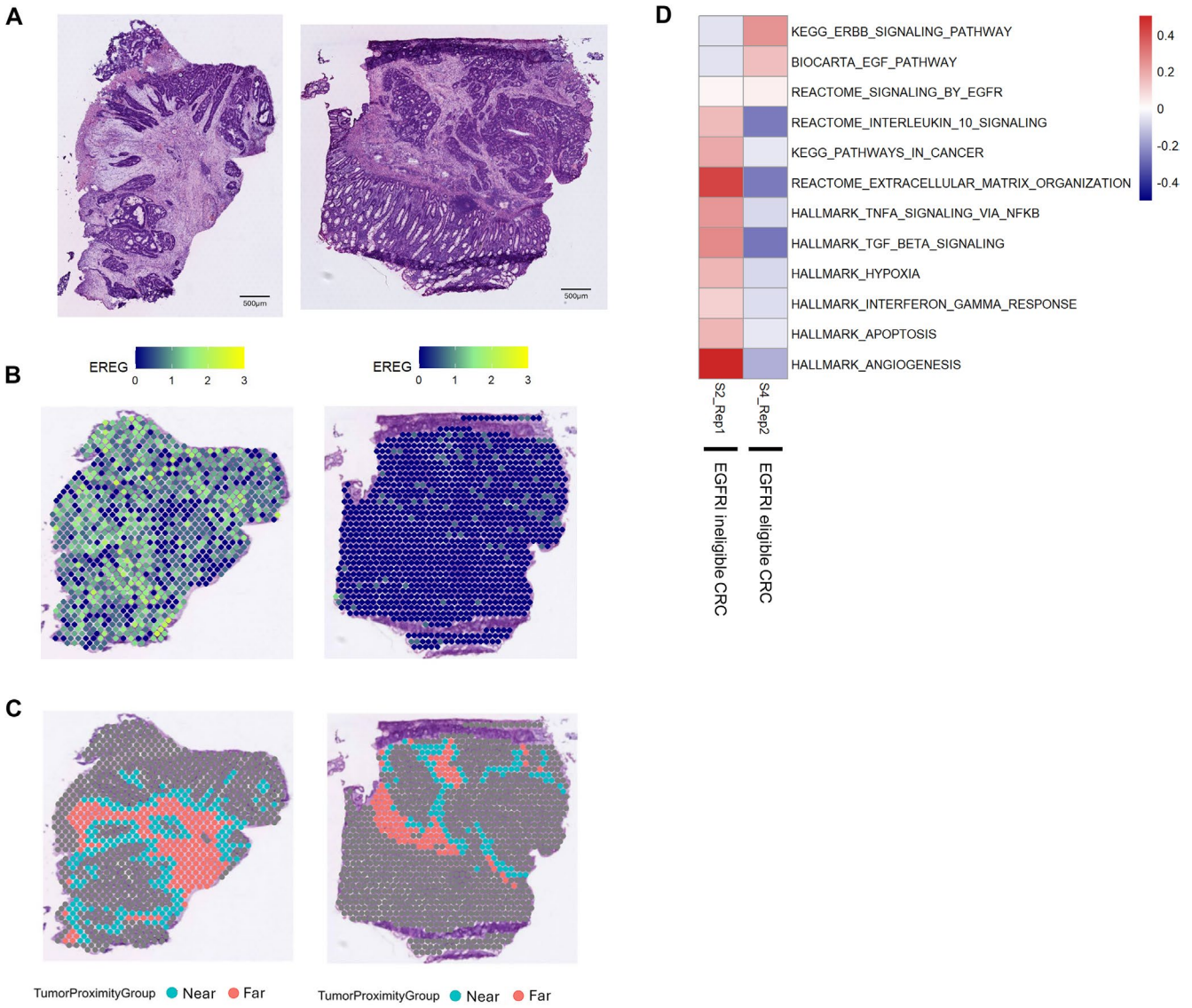

FIGURE 6 | Spatial transcriptomics reveals spatial interactions of CAF and TAM subtypes. (A) H&E staining images from representative EGFRI eligible (left panel) and ineligible (right panel) cases. Scale bar: 500 μm. (B) Spatial expression pattern of EREG in each case. (C, D) Comparison of pathway activity in stromal/immune spots based on proximity to cancer cells. (C) Representative spot classification (Near vs. Far). (D) Heatmap showing $\log_2$ fold change of pathway activity (Near vs. Far) in EGFRI-eligible (S4) and ineligible (S2) cases. Red indicates enriched activity near cancer cells.

and the proximal activation of the EGFR pathway exclusively in eligible cases.

This result supports that in EGFRI eligible cases, factors such as EREG expressed by cancer cells act on spatially proximal stromal-immune cell clusters (particularly those containing CAFs and TAMs), locally activating the EGFR pathway. The spatial transcriptomics findings corroborate that the "EREG/EGFR/CSF axis" identified through scRNA-seq analysis functions within specific spatial niches in the actual tumor tissue.

4 | Discussion

This study investigated CRC cases clinically eligible for EGFRI therapy (left-sided, BRAF wild-type, MSS) using integrated multi-transcriptomics to explore TME intercellular networks linked to sidedness and EGFRI eligibility. We found "EGFRI eligibility" better reflects cancer cell and TME characteristics than "sidedness" alone, uncovering biological bases for clinical differences. Crucially, we identified a specific "EREG/EGFR/CSF axis" in EGFRI eligible cases, driven by cancer cell-derived EREG and engaging non-myCAF and TAM/TAMo.

While sidedness is a key clinical indicator for EGFRI efficacy in RAS wild-type LCRC, underlying TME mechanisms are unclear, with prior research often focusing on cancer cell intrinsic features. Our study's novelty is using computational methods (CellChat, NicheNet) on multi-transcriptomic data to show EREG not just as a cancer cell factor, but as an initiator of a TME signaling cascade. We propose a multicellular network where cancer cell-derived EREG activates EGFR on nearby CAFs,

inducing CSF gene expression; these CSFs then target myeloid cells, offering new insights into biological distinctions linked to sidedness.

Regarding CAFs, suggested to play a central role in our findings, several key points warrant discussion. We classified CAFs into subtypes such as myCAF, iCAF, SOX6+ Fib, and ADAMDEC1+ Fib; among these, non-myCAFs were predicted to express EGFR and receive EREG signals. This finding is particularly interesting because, in many other cancer types, including pancreatic, breast, and lung cancer, CAFs are widely known to function primarily as producers and secretors of EGFR ligands [38–43]. Reports describing CAFs acting as recipients of cancer cell-derived EREG, as observed in our study, are scarce. This may indicate a unique CRC signaling modality, possibly where high local EREG concentrations induce EGFR signaling in CAFs that usually produce ligands, highlighting CAF functional diversity within the TME.

Considering that SOX6+ Fib and ADAMDEC1+ Fib might be gastrointestinal-specific fibroblasts [44, 45], elucidating the diverse roles of organ-specific fibroblasts and how they contribute functionally within the "EREG/EGFR/CSF axis" remains an important future challenge.

Whether the non-myCAFs identified as recipients of EREG signaling in this study actually enhance CSF production is currently supported only by indirect evidence, such as AP-1 via NicheNet and observed EGFR pathway activation in spatial analyses. This represents a limitation of the present study, and direct confirmation through future in vitro and in vivo functional experiments is warranted.

In conclusion, this study first demonstrates that within the TME of CRC associated with EGFRI eligibility, cancer cell-derived EREG drives a specific intercellular interaction network, the "EREG/EGFR/CSF axis," mediated through non-myCAFs and TAM/TAMo. This suggests a notable involvement of the EGFR pathway not only in cancer cells but also within the broader TME of these eligible tumors, rather than a full "addiction" at this stage. This discovery deepens our understanding of the mechanisms underlying EGFRI sensitivity in CRC and provides a crucial foundation for developing more refined patient stratification methods and novel therapeutic strategies that complement and potentially enhance classifications based on tumor sidedness.

Author Contributions

Atsuki Taniguchi: conceptualization, methodology, investigation, writing – original draft, funding acquisition. **Shunsuke Kagawa:** conceptualization, methodology, writing – review and editing, supervision. **Shohei Nogi:** investigation. **Tomohiko Yagi:** investigation. **Nobuhiko Kanaya:** supervision. **Shinji Kuroda:** supervision. **Satoru Kikuchi:** supervision. **Yoshihiko Kakiuchi:** supervision. **Hiroshi Tazawa:** methodology, supervision. **Toshiyoshi Fujiwara:** conceptualization, writing – review and editing, supervision.

Acknowledgments

Super-computing resources were provided by the Human Genome Center, the Institute of Medical Science, and the University of Tokyo.

Funding

This work was supported by the Japan Society for the Promotion of Science [KAKENHI Grant Number: 24K23359].

Ethics Statement

The authors have nothing to report.

Consent

The authors have nothing to report.

Conflicts of Interest

The authors declare no conflicts of interest.

Data Availability Statement

scRNA-seq datasets analyzed in this study are publicly available from the GEO (GSE200997) and the Synapse platform (ID syn26844071). Visium spatial transcriptomics data have been deposited on Zenodo (DOI: 10.5281/zenodo.7551712) and GSE226997. The Cancer Genome Atlas (TCGA) Colon Adenocarcinoma (COAD) and Rectum Adenocarcinoma (READ) project data (RNA sequencing and somatic mutation) were obtained from the Genomic Data Commons (GDC) portal. The custom analysis code is maintained on GitHub at [https://github.com/AtsukiTani/EREG-CRC].

References

1. P. Favoriti, G. Carbone, M. Greco, F. Pirozzi, R. E. Pirozzi, and F. Corcione, "Worldwide Burden of Colorectal Cancer: A Review," *Updates in Surgery* 68 (2016): 7–11, https://doi.org/10.1007/s13304-016-0359-y.

2. M. E. Salem, B. A. Weinberg, J. Xiu, et al., "Comparative Molecular Analyses of Left-Sided Colon, Right-Sided Colon, and Rectal Cancers," *Oncotarget* 8 (2017): 86356–86368, https://doi.org/10.18632/oncotarget.21169.

3. M. S. Lee, D. G. Menter, and S. Kopetz, "Right Versus Left Colon Cancer Biology: Integrating the Consensus Molecular Subtypes," *Journal of the National Comprehensive Cancer Network* 15 (2017): 411–419, https://doi.org/10.6004/jnccn.2017.0038.

4. W. Hu, Y. Yang, X. Li, et al., "Multi-Omics Approach Reveals Distinct Differences in Left- and Right-Sided Colon Cancer," *Molecular Cancer Research* 16 (2018): 476–485, https://doi.org/10.1158/1541-7786.Mcr-17-0483.

5. B. Flemer, D. B. Lynch, J. M. Brown, et al., "Tumour-Associated and Non-Tumour-Associated Microbiota in Colorectal Cancer," *Gut* 66 (2017): 633–643, https://doi.org/10.1136/gutjnl-2015-309595.

6. J. M. Lee, Y. D. Han, M. S. Cho, et al., "Impact of Tumor Sidedness on Survival and Recurrence Patterns in Colon Cancer Patients," *Annals of Surgical Treatment and Research* 96 (2019): 296–304, https://doi.org/10.4174/astr.2019.96.6.296.

7. D. R. Lim, J. K. Kuk, T. Kim, and E. J. Shin, "Comparison of Oncological Outcomes of Right-Sided Colon Cancer Versus Left-Sided Colon Cancer After Curative Resection: Which Side Is Better Outcome?," *Medicine* 96 (2017): e8241, https://doi.org/10.1097/md.0000000000008241.

8. F. Loupakis, D. Yang, L. Yau, et al., "Primary Tumor Location as a Prognostic Factor in Metastatic Colorectal Cancer," *Journal of the National Cancer Institute* 107 (2015): dju427, https://doi.org/10.1093/jnci/dju427.

9. D. Rossini, A. Boccaccino, M. Carullo, et al., "Primary Tumour Side as a Driver for Treatment Choice in RAS Wild-Type Metastatic Colorectal Cancer Patients: A Systematic Review and Pooled Analysis of

Randomised Trials," *European Journal of Cancer* 184 (2023): 106–116, https://doi.org/10.1016/j.ejca.2023.02.006.

10. A. Cervantes, R. Adam, S. Roselló, et al., "Metastatic Colorectal Cancer: ESMO Clinical Practice Guideline for Diagnosis, Treatment and Follow-Up," *Annals of Oncology* 34 (2023): 10–32, https://doi.org/10.1016/j.annonc.2022.10.003.

11. V. K. Morris, E. B. Kennedy, N. N. Baxter, et al., "Treatment of Metastatic Colorectal Cancer: ASCO Guideline," *Journal of Clinical Oncology* 41 (2023): 678–700, https://doi.org/10.1200/jco.22.01690.

12. D. Arnold, B. Lueza, J. Y. Douillard, et al., "Prognostic and Predictive Value of Primary Tumour Side in Patients With RAS Wild-Type Metastatic Colorectal Cancer Treated With Chemotherapy and EGFR Directed Antibodies in Six Randomized Trials," *Annals of Oncology* 28 (2017): 1713–1729, https://doi.org/10.1093/annonc/mdx175.

13. A. Stahler, S. Stintzing, D. P. Modest, et al., "Amphiregulin Expression Is a Predictive Biomarker for EGFR Inhibition in Metastatic Colorectal Cancer: Combined Analysis of Three Randomized Trials," *Clinical Cancer Research* 26 (2020): 6559–6567, https://doi.org/10.1158/1078-0432.Ccr-20-2748.

14. C. J. M. Williams, F. Elliott, N. Sapanara, et al., "Associations Between AI-Assisted Tumor Amphiregulin and Epiregulin IHC and Outcomes From Anti-EGFR Therapy in the Routine Management of Metastatic Colorectal Cancer," *Clinical Cancer Research* 29 (2023): 4153–4165, https://doi.org/10.1158/1078-0432.Ccr-23-0859.

15. C. M. Garvey, R. Lau, A. Sanchez, et al., "Anti-EGFR Therapy Induces EGF Secretion by Cancer-Associated Fibroblasts to Confer Colorectal Cancer Chemoresistance," *Cancers (Basel)* 12 (2020): 1393, https://doi.org/10.3390/cancers12061393.

16. J. Zhou, Q. Ji, and Q. Li, "Resistance to Anti-EGFR Therapies in Metastatic Colorectal Cancer: Underlying Mechanisms and Reversal Strategies," *Journal of Experimental & Clinical Cancer Research* 40 (2021): 328, https://doi.org/10.1186/s13046-021-02130-2.

17. D. M. Muzny, M. N. Bainbridge, K. Chang, et al., "Comprehensive Molecular Characterization of Human Colon and Rectal Cancer," *Nature* 487 (2012): 330–337, https://doi.org/10.1038/nature11252.

18. T. G. Araújo, S. T. S. Mota, H. S. V. Ferreira, M. A. Ribeiro, L. R. Goulart, and L. Vecchi, "Annexin A1 as a Regulator of Immune Response in Cancer," *Cells* 10 (2021): 2245, https://doi.org/10.3390/cells10092245.

19. H. Hosseinalizadeh, Q. M. Hussain, Z. Poshtchaman, et al., "Emerging Insights Into Keratin 7 Roles in Tumor Progression and Metastasis of Cancers," *Frontiers in Oncology* 13 (2023): 1243871, https://doi.org/10.3389/fonc.2023.1243871.

20. J. D. G. Leach, N. Vlahov, P. Tsantoulis, et al., "Oncogenic BRAF, Unrestrained by TGFβ-Receptor Signalling, Drives Right-Sided Colonic Tumorigenesis," *Nature Communications* 12 (2021): 3464, https://doi.org/10.1038/s41467-021-23717-5.

21. A. M. Newman, C. B. Steen, C. L. Liu, et al., "Determining Cell Type Abundance and Expression From Bulk Tissues With Digital Cytometry," *Nature Biotechnology* 37 (2019): 773–782, https://doi.org/10.1038/s41587-019-0114-2.

22. M. S. Lee, E. J. McGuffey, J. S. Morris, et al., "Association of CpG Island Methylator Phenotype and EREG/AREG Methylation and Expression in Colorectal Cancer," *British Journal of Cancer* 114 (2016): 1352–1361, https://doi.org/10.1038/bjc.2016.87.

23. J. Jacob, Y. Anami, P. C. High, et al., "Antibody–Drug Conjugates Targeting the EGFR Ligand Epiregulin Elicit Robust Antitumor Activity in Colorectal Cancer," *Cancer Research* 85 (2025): 973–986, https://doi.org/10.1158/0008-5472.Can-24-0798.

24. S. Jin, C. F. Guerrero-Juarez, L. Zhang, et al., "Inference and Analysis of Cell-Cell Communication Using CellChat," *Nature Communications* 12 (2021): 1088, https://doi.org/10.1038/s41467-021-21246-9.

25. S. Jin, M. V. Plikus, and Q. Nie, "CellChat for Systematic Analysis of Cell–Cell Communication From Single-Cell Transcriptomics," *Nature Protocols* 20 (2025): 180–219, https://doi.org/10.1038/s41596-024-01045-4.

26. R. Browaeys, W. Saelens, and Y. Saeys, "NicheNet: Modeling Intercellular Communication by Linking Ligands to Target Genes," *Nature Methods* 17 (2020): 159–162, https://doi.org/10.1038/s41592-019-0667-5.

27. F. Mascia, C. Cataisson, T. C. Lee, et al., "EGFR Regulates the Expression of Keratinocyte-Derived Granulocyte/Macrophage Colony-Stimulating Factor In Vitro and In Vivo," *Journal of Investigative Dermatology* 130 (2010): 682–693, https://doi.org/10.1038/jid.2009.336.

28. M. Harrington, B. W. Konicek, X. L. Xia, and A. Song, "Transcriptional Regulation of the Mouse CSF-1 Gene," *Molecular Reproduction and Development* 46 (1997): 39–44; discussion 44–35, https://doi.org/10.1002/(sici)1098-2795(199701)46:1<39::Aid-mrd7>3.0.Co;2-s.

29. N. Ye, Y. Ding, C. Wild, Q. Shen, and J. Zhou, "Small Molecule Inhibitors Targeting Activator Protein 1 (AP-1)," *Journal of Medicinal Chemistry* 57 (2014): 6930–6948, https://doi.org/10.1021/jm5004733.

30. E. Elyada, M. Bolisetty, P. Laise, et al., "Cross-Species Single-Cell Analysis of Pancreatic Ductal Adenocarcinoma Reveals Antigen-Presenting Cancer-Associated Fibroblasts," *Cancer Discovery* 9 (2019): 1102–1123, https://doi.org/10.1158/2159-8290.Cd-19-0094.

31. Y. Kieffer, H. R. Hocine, G. Gentric, et al., "Single-Cell Analysis Reveals Fibroblast Clusters Linked to Immunotherapy Resistance in Cancer," *Cancer Discovery* 10 (2020): 1330–1351, https://doi.org/10.1158/2159-8290.Cd-19-1384.

32. K. Pelka, M. Hofree, J. H. Chen, et al., "Spatially Organized Multicellular Immune Hubs in Human Colorectal Cancer," *Cell* 184 (2021): 4734–4752.e4720, https://doi.org/10.1016/j.cell.2021.08.003.

33. J. Qian, S. Olbrecht, B. Boeckx, et al., "A Pan-Cancer Blueprint of the Heterogeneous Tumor Microenvironment Revealed by Single-Cell Profiling," *Cell Research* 30 (2020): 745–762, https://doi.org/10.1038/s41422-020-0355-0.

34. D. A. Hume, K. M. Summers, C. O'Brien, and P. Pavli, "The Relationship Between CSF1R Signaling, Monocyte-Macrophage Differentiation, and Susceptibility to Inflammatory Bowel Disease," *Cellular and Molecular Gastroenterology and Hepatology* 19 (2025): 101510, https://doi.org/10.1016/j.jcmgh.2025.101510.

35. E. Azizi, A. J. Carr, G. Plitas, et al., "Single-Cell Map of Diverse Immune Phenotypes in the Breast Tumor Microenvironment," *Cell* 174 (2018): 1293–1308.e1236, https://doi.org/10.1016/j.cell.2018.05.060.

36. C. V. Jones and S. D. Ricardo, "Macrophages and CSF-1: Implications for Development and Beyond," *Organogenesis* 9 (2013): 249–260, https://doi.org/10.4161/org.25676.

37. M. R. Vahid, E. L. Brown, C. B. Steen, et al., "High-Resolution Alignment of Single-Cell and Spatial Transcriptomes With CytoSPACE," *Nature Biotechnology* 41 (2023): 1543–1548, https://doi.org/10.1038/s41587-023-01697-9.

38. G. Mucciolo, J. Araos Henríquez, M. Jihad, et al., "EGFR-Activated Myofibroblasts Promote Metastasis of Pancreatic Cancer," *Cancer Cell* 42 (2024): 101–118.

39. T. Murata, H. Mizushima, I. Chinen, et al., "HB-EGF and PDGF Mediate Reciprocal Interactions of Carcinoma Cells With Cancer-Associated Fibroblasts to Support Progression of Uterine Cervical Cancers," *Cancer Research* 71 (2011): 6633–6642.

40. T. Nakanishi, Y. I. Koma, S. Miyako, et al., "AREG Upregulation in Cancer Cells via Direct Interaction With Cancer-Associated Fibroblasts Promotes Esophageal Squamous Cell Carcinoma Progression Through EGFR-Erk/p38 MAPK Signaling," *Cells* 13 (2024): 1733.

41. F. B. Rahman, Y. Kadowaki, S. Ishihara, et al., "Fibroblast-Derived HB-EGF Promotes Cdx2 Expression in Esophageal Squamous Cells," *Laboratory Investigation* 90 (2010): 1033–1048.

42. G. Su, K. E. Sung, D. J. Beebe, and A. Friedl, "Functional Screen of Paracrine Signals in Breast Carcinoma Fibroblasts," *PLoS One* 7 (2012): e46685.

43. Q. Xu, Q. Long, D. Zhu, et al., "Targeting Amphiregulin (AREG) Derived From Senescent Stromal Cells Diminishes Cancer Resistance and Averts Programmed Cell Death 1 Ligand (PD-L1)-Mediated Immunosuppression," *Aging Cell* 18 (2019): e13027.

44. Y. Gao, J. Li, W. Cheng, et al., "Cross-Tissue Human Fibroblast Atlas Reveals Myofibroblast Subtypes With Distinct Roles in Immune Modulation," *Cancer Cell* 42 (2024): 1764–1783.e1710, https://doi.org/10.1016/j.ccell.2024.08.020.

45. J. Kinchen, H. H. Chen, K. Parikh, et al., "Structural Remodeling of the Human Colonic Mesenchyme in Inflammatory Bowel Disease," *Cell* 175 (2018): 372–386.e317, https://doi.org/10.1016/j.cell.2018.08.067.

Supporting Information

Additional supporting information can be found online in the Supporting Information section. **Figure S1.** (A) Stacked bar plot showing the proportional distribution of major cell types across the six integrated scRNA-seq datasets. (B) Dot plot illustrating the expression levels of EREG in cancer cells across the different datasets. **Figure S2.** (A) FeaturePlot visualization of the expression of mucinous cancer-associated genes (REG4, SPINK4, FCGBP, MUC2). (B–D) Pseudo-bulk PCA of major non-cancer cell types stratified by EGFRI eligibility. Fibroblasts (B), T cells (C), Myeloid cells (D). **Figure S3.** (A) Heatmap showing DEGs in cancer cells identified based on EGFRI eligibility. (B) Dot plot of other major EGFR ligand expression in cancer cells, stratified by RAS status and sidedness. (C) Comparison of the number of intercellular interactions between EGFRI eligible and ineligible cases using CellChat. Heatmap shows relative cell–cell communication strength in eligible versus ineligible cases (rows: sender cells, columns: receiver cells). (D) Visualization of differential relative information flow in pathways between EGFRI eligible and ineligible cases using CellChat. Signaling pathways from cancer cells to fibroblasts (left panel). Signaling pathways from fibroblasts to myeloid cells (right panel). (E) Bubble plots comparing the communication probabilities of specific ligand receptor (L-R) pairs in EGF and CSF signaling pathways between EGFRI eligible and ineligible cases. (F) Scatter plot showing the Spearman correlation between pseudobulk expression levels of EREG in cancer cells and CSF1 in fibroblasts across individual samples. **Figure S4.** (A) FeaturePlot showing the expression of representative CAF marker genes (ACTA2, FAP, RGS5, SOX6, CSF1, ADAMDEC1). (B) FeaturePlot showing iCAF score (left panel) and myCAF score (right panel) calculated using AddModuleScore function. **Figure S5.** (A) FeaturePlot showing the expression of TAM-associated marker genes (CD163, MRC1, S100A8, TREM2, SPP1, CSF1R) and neutrophil-specific markers (MPO, CEACAM8, FCGR3B), confirming the absence of neutrophil contamination. (B) Expression of EGFR ligands in TAM/TAMo subtypes. AREG (left panel). EREG (right panel). **Figure S6.** (A) Spatial cell composition estimation using CytoSPACE. Stacked bar plot showing the estimated abundance of cell types. (B) Spatial distribution of signature scores for major cell types (epithelial cells, fibroblasts, myeloid cells). EGFR eligible case (top row), EGFR ineligible case (bottom row). (C) Validation of spatial distribution using an independent Visium cohort (GSE226997). Spatial feature plots display signature scores for major cell types and EREG expression across three cases: P1 (Eligible), P2 (Ineligible), and P4 (Ineligible). (D) Heatmap showing the log2 fold change of AUCell derived pathway activity scores in stromal spots located near versus far from tumor cells in the GSE226997 cohort (P1 and P2). Case P4 (Ineligible) was excluded from this proximity based pathway analysis because the tumor developed within an adenoma, and spots annotated computationally as epithelial cells could not be strictly defined as cancer cells. **Table S1.** scRNA-seq samples. **Table S2.** ST samples.